

**ROSAT, ASCA AND OSSE OBSERVATIONS OF THE
BROAD LINE RADIO GALAXY 3C120**

P. Grandi¹, R. M. Sambruna², L. Maraschi³, G. Matt⁴,

C. M. Urry⁵, R. F. Mushotzky²

¹ Istituto di Astrofisica Spaziale - CNR, Via E. Fermi 21, I-00044 Frascati (Roma), Italy

² NASA/GSFC Code 662, Greenbelt, MD 20771

³ Osservatorio Astronomico di Brera, via Brera 28, I-20121 Milano, Italy

⁴ Dipartimento di Fisica, Universita' degli Studi "Roma Tre", Via della Vasca Navale 84,
I-00146 Roma, Italy

⁵ Space Telescope Science Institute, 3700 San Martin Drive, Baltimore, MD 21218

Received _____; accepted _____

ABSTRACT

We present simultaneous observations of the superluminal radio galaxy 3C 120 performed with the ASCA and GRO (OSSE) satellites on February-March 1994, as well as an analysis of all the ROSAT archival data. The ASCA spectrum of this object can be described by an absorbed ($N_H = 1.6 \times 10^{21} \text{cm}^{-2}$) power law with photon index $\Gamma_{ASCA} = 2$ and a very broad ($\sigma > 0.8 \text{ keV}$) intense iron line ($EW > 400 \text{ eV}$) at $\sim 6 \text{ keV}$.

The combined ASCA–OSSE data do not exclude the presence of a narrower ($\sigma = 0.4 \text{ keV}$) and less intense ($EW < 300 \text{ eV}$) iron line plus a hard component, corresponding either to reflection from an accretion disk or to a flatter power law from a jet. However a single power law plus broad Fe line is preferred from a statistical point of view by the ASCA data

The ROSAT data yield a column density in excess of the Galactic value. The spectral slopes, ranging from $\Gamma_{ROSAT} = 2.5$ to 3.3, are steeper than that measured by ASCA, suggesting the presence of a soft excess. The 0.1-2 keV power-law slope is variable and softer at higher intensity.

These results show that the combined soft and hard X-ray spectrum of 3C 120 is rather complex. The intrinsic absorption, the soft excess, and the iron line indicate that the X-ray emission from this blazar-like radio galaxy is dominated by a Seyfert-like component, at least in the 0.1-10 keV energy band. The jet contribution, if present, becomes important only at higher energies.

Subject headings: galaxies: nuclei – Radio Galaxy – X-ray spectra

1. Introduction

3C 120 is a relatively nearby ($z=0.033$) core-dominated broad-line radio galaxy with a superluminal jet extending from 0.5 pc to 100 kpc and diffuse radio structures in several directions (Walker et al. 1987). A faint optical counterpart of the radio jet has recently been detected in deep high-resolution images (Hjorth et al. 1995).

Although 3C 120 is classified as a Seyfert 1 galaxy, its optical morphology is not simple. Photometric and spectroscopic studies of the weak nebulosity around the nucleus indicate the presence of two components, a spheroidal system plus an extended disk, which suggests 3C 120 may have resulted from the merging of two different galaxies (Moles et al. 1988). The indication of a possible double nucleus in monochromatic emission line images (Hua 1988) and the observation of extended, strongly perturbed emission line regions (Tadhunter et al. 1989; Baum, Heckman, & van Breugel 1992) support this hypothesis. The origin of the photons ionizing the extended emission-line regions is still debated; the photoionizing flux may derive from the nuclear AGN continuum, or from the interaction of the jet with the interstellar medium, or from local young stars (Baldwin et al. 1980, Balick & Heckman 1979, Hua 1988, Moles et al. 1988)

At UV wavelengths, 3C 120 has a typical AGN spectrum with a strong blue bump and strong emission lines (Maraschi et al. 1991, hereafter M91). In the X-ray band, a simple absorbed power law gave an adequate representation of the EXOSAT spectrum (M91). No soft excess was detected with EXOSAT, while earlier *Einstein* Solid State Spectrometer (SSS) data indicated the presence of emission lines at low energies (Petre et al. 1984, Turner et al. 1991). No information about the iron line at 6.4 keV or possible Compton reflection from a disk was available before the ASCA observations because 3C 120 was never observed with Ginga. At higher energies, it has been detected several times in the energy band 50-150 keV with OSSE (Johnson et al. 1994), but never at MeV or higher energies

with Comptel or EGRET (Maisak et al. 1995, von Montigny et al. 1995).

The X-ray spectral variability of 3C 120 is unusual. The energy spectral index in the 0.3-6 keV band, measured with EXOSAT, varied between $\alpha \sim 0.5$ and $\alpha \sim 0.8 - 1$ and was positively correlated with the soft luminosity, but uncorrelated with the hard luminosity (M91). A possible interpretation of this behavior is that the beamed radiation from the jet contributes only to the hard X-ray emission. Seyferts generally become softer when the X-ray luminosity increases, while blazars, dominated by jet emission, become harder as their intensity increases (Giommi et al. 1989; Grandi et al. 1992, Sambruna et al. 1994).

The detection of thermal features in the X-ray spectrum of 3C 120 is a very important diagnostic of the presence of nonthermal emission from the jet. The featureless beamed X-ray continuum will tend to dilute any spectral features, such as absorption edges or emission lines often found in Seyfert galaxies, when its relative contribution is important. In this regard, no conclusions could be derived up to now because of the lack of data with sufficient sensitivity at both soft and hard X-ray energies.

Motivated by the complexity of this radio galaxy, we organized simultaneous observations of 3C 120 with ASCA and OSSE-GRO covering the energy range 0.5–150 keV. Archival ROSAT PSPC data of this source, covering the energy range 0.05–2.0 keV, were also analyzed. With such broad energy coverage, we have for the first time the possibility of strongly constraining the X-ray emission mechanisms and understanding more about the innermost structure in 3C 120.

2. ASCA Observations

2.1. Observations and Data Analysis

We observed 3C 120 with ASCA for 50,000 sec on 1994 February 17-19 (the journal of the observations is given in Table 1). The two Solid-state Imaging Spectrometers (SIS0,SIS1) operated in faint mode during the observation, with only one CCD used (1-CCD mode) and the two Gas Imaging Spectrometers (GIS2,GIS3) in Pulse Height mode. The average source flux during the pointing was $F_{2-6 \text{ keV}} \sim 3 \times 10^{-11} \text{ ergs cm}^{-2} \text{ s}^{-1}$. Compared to the measured EXOSAT fluxes (M91), 3C 120 was in an intermediate brightness state during our ASCA observation.

Data reduction for all 4 instruments on ASCA (SIS0, SIS1, GIS2, GIS3; Tanaka, Inoue, & Holt 1994) followed the standard procedures in the ABC Guide (Day et al. 1994). Specifically, screening criteria include the rejection of data taken during intervals of Earth and elevation angles lower than 20° and 10° , respectively, and magnetic rigidity lower than 6 GeV/c for the SIS detectors and 10 GeV/c for the GIS detectors. Data taken during passage through the South Atlantic anomaly were also rejected.

The SIS and GIS spectra were accumulated on circular regions centered on the source position with radii 4 arcmin and 6 arcmin, respectively, due to the different point-spread functions of the two instruments. The GIS background was calculated from the same source image, while the SIS background from blank-sky observations (available from the ASCA Guest Observer Facilities). In the SIS case, we opted for blank sky observations because the brightness of the source and the broad PSF strongly reduced the regions where the local background could be measured. In both cases, the background spectrum was accumulated within regions having the same dimensions as the source circle and from blank-sky.

The spectra were rebinned in order to have at least 20 counts per new bin, to validate the use of the χ^2 statistic in the spectral fits. The more recent versions (1994 November 9) of the standard redistribution matrices (RMF) of the SIS and GIS were taken from the

ASCA Calibration Database on the public node `legacy.gsfc.nasa.gov`, while the ancillary files (ARF) have been appropriately built for each instrument with the program ‘`ascaarf`’ (version 2.62) of the FTOOLS package. Spectral fits were performed using the XSPEC package.

For each instrument, light curves with different bin size (100, 500, 1000 sec) were extracted in XSELECT and analyzed using the XRONOS package.

2.2. Timing Analysis

Significant time variability was detected in all the instruments, in agreement with the findings of Nandra et al. (1996a) for 3C120. A clear increasing trend is present in both the SISs and GISs, the flux changing $\sim 30\%$ during the observation (see Figures 1a-1b). A standard χ^2 test, applied to the average count rate in each light curve, confirms the variability of 3C 120: the probability that the source was constant is less than 10^{-3} in both the SISs and GISs light curves, independent of the bin size used. The χ^2 values are listed in Table 2 for each instrument and for each bin size.

2.3. Spectral Fits

We performed spectral fits on data from the individual and combined instruments. Since we did not find significant differences, we discuss here only the results from the combined instruments (SIS0+SIS1, GIS2+GIS3, and SIS0+SIS1+GIS2+GIS3).

The spectral fit parameters are reported in Table 3. The listed uncertainties correspond to the 90% confidence interval for one parameter of interest ($\Delta\chi^2 = 2.7$). When the parameters are not well constrained by XSPEC, we report only an upper limit.

We first fitted the SIS data in a soft band, 0.6-5 keV, to avoid the complexity in the Fe spectral region. Because of the uncertain SIS calibration at low energies, we excluded the data below 0.6 keV. A single absorbed power law with $\Gamma = 2.00 \pm 0.02$ and $N_H = 1.64(\pm 0.07) \times 10^{21} \text{ cm}^{-2}$ is sufficient to fit the SIS spectra very well (see table 3). The fitted column density is consistent with Galactic $N_H^{\text{Gal}} = 1.23 \times 10^{21} \text{ cm}^{-2}$ (Elvis et al. 1989), especially allowing for the systematic SIS overestimate of $N_H = 2\text{-}3 \times 10^{20} \text{ cm}^{-2}$.

In order to investigate the hard X-ray emission of 3C 120, the spectral fits were then extended to energies > 5 keV. We fitted the SIS data from 0.6 to 8 keV and the GIS data from 1 to 10 keV. A single absorbed power law gives an unacceptable χ^2 both for the two SISs and GISs (Table 3) with residuals showing an excess around 6 keV (Fig. 2a-2b). When a Gaussian emission line is included in the model, the χ^2 improves significantly (the F-test indicates the addition of two parameters represents an improvement at a confidence level $> 99\%$ for both the SIS and GIS data.) We alternately added a Gaussian emission line to a power law with fixed slope ($\Gamma = 2$, as suggested by the soft spectrum) and to a power law with free slope. The results are similar, but obviously the uncertainties are smaller in the first case. The position of the line ($E_{Fe} = 6.06_{-0.21}^{+0.26}$ in SISs and $E_{Fe} = 6.30_{-0.19}^{+0.20}$ in GISs) is consistent, within the uncertainties, with fluorescent iron from cold matter (observed $E_{FeK\alpha} = 6.4/1.033 = 6.196$ keV).

The iron line is unambiguously detected at 99% confidence, as shown in Figure 3 where the confidence contours of the line width versus the line normalization are plotted for a power law with Γ free to vary.

The observed intrinsic width of the line ($\sigma \sim 0.8 - 1$ keV) and its equivalent width (EW > 400 eV) are rather large. (The Gaussian fitted to the combined GIS spectra is somewhat larger than that for the two SIS, probably because of the different energy resolution and ranges covered by the instruments.) We investigated different possibilities

for the line broadening. We first tested an emission profile from a relativistic disk around a Schwarzschild black hole (Fabian et al. 1989). We fitted the higher-resolution SIS data with a power law with fixed slope ($\Gamma = 2$) illuminating an accretion disk with inner and outer radii $r_i = 10$ and $r_o = 1000$ (in units of GM/c^2). The inclination of the disk was fixed at $i = 15^\circ$; this is the upper limit of the angle to the line of sight for the radio jet, as deduced from its apparent superluminal velocity $\beta_{app} \sim 8$ (Zensus 1989). As shown in Table 3, for the constrained inclination angle the χ_r^2 is worse for the diskline model than the gaussian line model. A low-inclination disk can not account for the observed emission line. Relaxing the inclination angle, the model fit requires a viewing angle close to 90° , which is difficult to reconcile with the superluminal properties of the jet (if orthogonal to the disk) and with the brightness of the blue bump.

The broad Gaussian profile of the iron line is also preferred to a blending of two narrow lines. Two Gaussian profiles with narrow fixed intrinsic widths ($\sigma_1 = \sigma_2 = 0.1$ keV) can not adequately reproduce the SIS emission feature (see Table 3). When we allowed the widths to vary, the fitted normalization of one of the two Gaussians converges to zero.

We checked whether the addition of a hard component could change the X-ray continuum shape and affect the iron line in both the SIS and GIS data. Two different models were used, (i) a Compton reflection and (ii) a broken power law. A reflection model is directly suggested by the presence of the K_α line (Lightman & White 1988, Matt et al. 1991, George & Fabian 1991). A flatter second power law is expected if the jet contributes to the X-ray spectrum. We parameterized the reflection component using the PLREF model in XSPEC. It assumes the illumination of a cold disk from an X-ray source and uses the Lightman and White (1988) approximation to calculate the shape of the reflected spectrum.

- (i) In order to better constrain the hard component, the power-law slope was frozen at

$\Gamma = 2$ and all the input parameters, except the ratio (R) between the normalization of the power law and the reflection component, were fixed to the default values.

A Gaussian centered at 6.2 keV and with intrinsic width 0.4 keV (a “standard” iron line shape, as suggested by Nandra et al. 1996b) was added, with parameters fixed at first and then free to vary. As shown in Table 3, the hard component ($R = 0.8$ and $R = 1.6$ in the SIS and in the GIS, respectively) contributed to the continuum and reduced the EW of the line if the Gaussian profile was defined “a priori”, but it was not necessary anymore ($R < 0.44$) if the iron line parameters were free to vary. In this latter case the line is again very broad.

This result reveals that the amount of reflection and the line parameters are strongly correlated. This is clearly shown in Figure 4 where the GIS2+GIS3 probability contours of the line width versus (σ) versus the ratio (R) between the normalization of the power law and the reflection component are plotted.

(ii) Similar results were obtained fitting the data with two power laws plus a Gaussian. If the energy and the intrinsic width of the line were frozen ($\sigma = 0.4$ keV), the power law was significantly flatter above the energy break (estimated around ~ 4 keV) and the iron equivalent width was small. If we allowed the line to broaden, the hard power-law slope became steeper (the photon index became comparable to the value below the break) and the EW of the line increased again. Simultaneous fits to all four instruments confirm these results (Table 3). In this case, we obtained only an upper limit for the normalization of the reflected component if the iron line profile is gaussian.

We then conclude that it is not possible with the ASCA data alone to constrain the contribution of a hard component that, if present, could affect the measured strength and profile of the line. The actual detection of an emission feature at 6.2 keV, however, does ensure that the contribution of the jet is small below ~ 8 keV.

3. OSSE Observations

3C 120 was observed with OSSE from February 17 to March 1 1994, overlapping with the ASCA observations. A shorter pointing was also performed a week later, from March 8 to March 15. The source was very faint. In both the observations, it was detected at only a 2σ level of significance ($c/s = 0.084 \pm 0.042$ and $c/s = 0.090 \pm 0.045$ in the first and second pointing, respectively). Because of this, we could not obtain an OSSE spectrum on February-March 1994, but only an average flux from the sum of both observations.

In order to constrain the shape of the high energy emission, the more plausible models for the ASCA data were extrapolated to 150 keV and compared to the observed OSSE flux. In particular we considered a simple power law plus a broad iron line, and a power law plus a hard component with a “standard” iron line shape. As can be seen in Figure 5, none of the models can be definitely rejected.

Using non-contemporaneous OSSE fluxes from literature, the high energy spectrum appears to be well fit by a harder model. In Figure 5, the open point represents the weighted average flux from all the 1992-1993 detections of 3C 120 in the 50-150 keV band (Johnson et al. 1994). In this case, however, the non-simultaneity of the ASCA and OSSE data limits our ability to constrain the ASCA extrapolation.

4. ROSAT Observations

3C 120 was observed with the ROSAT Positional Sensitive Proportional Counter (PSPC) in pointed mode on four separate occasions in March, September, and August 1993. The log of the observations is reported in Table 1. We analyzed the archival PSPC data using XSELECT. The events were corrected for spatial gain changes using the “pcsasscor” tool (ROSAT Status Report, No. 137, April 1, 1996). The data were extracted in a circle

centered on the target position and with radius 2 arcmin, which is large enough to collect all the softest photons from the source and avoid the “ghost-image” problem. The background was estimated in a circle of the same radius at ~ 4 arcmin away from the source. According to the WGA catalog (White, Giommi, & Angelini 1994), any serendipitous sources in the field of 3C 120 are too faint (< 0.01 c/s) to affect our analysis.

Source spectra were extracted in 256 PI channels and rebinned on the channel range 12-211 (energy range 0.15–2.1 keV) in order to have at least 20 counts per new bin. Since the observations were performed in low-gain mode (i.e., after October 1991), we used the `pspcb-gain2-256` matrix for the spectral fits, as appropriate.

4.1. Timing Analysis

The source intensity varied among the four observing epochs, from a minimum count rate in the energy range 0.1–2.1 keV of 1.74 ± 0.03 cts/s in March 1993 to a maximum count rate of 3.01 ± 0.04 cts/s in August 1993 (Table 1).

In order to test for variability of the flux within the single exposures, we applied the Kolmogorov-Smirnov (KS) test on unbinned data and the χ^2 test on binned data. Flux variability was detected for the 1993 September 10 observation, at 99% confidence according to the KS test. In order to apply the χ^2 test we rebinned the light curve on time scales ≥ 400 s, in order to avoid spurious variability due to the satellite wobble. The light curve with bins at 400 s is shown in Figure 6. Constant emission is ruled out at 99% confidence.

4.2. Spectral Fits

The ROSAT data were first fitted separately with a single power law with free N_H . The fit parameters are reported in Table 4 together with their 90% confidence uncertainties for

one parameter of interest.

In all cases the fitted absorption is significantly ($> 99\%$ confidence) higher than the Galactic value, $N_H^{\text{Gal}} = 1.23 \times 10^{21} \text{ cm}^{-2}$. This confirms previous results based on *Einstein* IPC and SSS data (Kruper, Urry, & Canizares 1990; Turner et al. 1991). The ROSAT data are characterized by a continuum with photon index $\Gamma=2.5\text{--}3.3$, systematically steeper than that measured at higher energies by ASCA ($\Delta\Gamma > 0.5$).

There is some evidence ($\sim 90\%$ confidence) for variation of the both spectral parameters with source intensity. The column density increases and the photon index gets steeper from March 6, when the source was fainter, to the brighter state of August 25. The steepening of the spectrum with increasing the soft intensity is consistent with the EXOSAT results (M91).

The difference between ASCA and ROSAT spectral slopes suggests the presence of a soft excess at low energies.

It is known that calibration problems affect the PSPC results: Fiore et al (1994) showed a systematic difference between IPC-Einstein and ROSAT-PSPC spectra of $\Delta\Gamma \sim 0.2$. However, we exclude that the discrepancies between ASCA and ROSAT results are only due to calibration problems. The ROSAT power laws are steeper than ASCA and always ≥ 0.5 . In addition the ASCA slope is well determined. It is measured over a large energy band and appears in good agreement with the previous results from HEA0-1, *Einstein*-MPC and EXOSAT (Rothschild et al. 1983, Treves et al. 1988, M91).

In order to model the soft excess, we added a Raymond Smith model to the simple power law and fixed N_H to the Galactic value (as suggested by ASCA data). The results are listed in Table 5. Acceptable χ^2 are obtained for all the epochs, but the additional component does not significantly improve the fit. However, the spectral indices in Table 5 are more close to the values usually observed at higher energies and the temperature

(0.6-0.8 keV) is in reasonable agreement with the result of Turner et al. (1991).

Summarizing, there is evidence in the ROSAT data of flux variability on both long (\sim months) and short (\sim minutes) time scales. There is evidence of a complex soft component. Spectral variability is confirmed, with the spectral slope getting steeper when the intensity increases.

5. Discussion and Conclusions

3C 120 is a variable and complex X-ray source. The Seyfert-like spectrum is characterized by a steep power law ($\Gamma = 2.0$), by an iron line from cold matter and by a probable soft excess. At higher energies (50-150 keV), our observations do not allow to strongly constrain the spectral shape. The OSSE measurements are consistent with a simple power law extrapolated by the ASCA data, but do not exclude the presence of an additional hard component.

In details, the major observational results of this study are as follows:

1. The ASCA data have revealed the presence of an iron line in 3C 120 for the first time. If the continuum is modeled with a single power law, the iron line is broader ($\sigma \sim 0.9$ keV) and more intense (~ 500 keV) than in most Seyfert 1 galaxies. An object with a similar and intense broad line is the Seyfert 2 galaxy, IRAS 1832 (Iwasawa et al. 1996).
2. A hard component (from a disk or jet) can fit the hard ASCA spectrum but is not required. However, the amount of reflection (or the jet contribution) anti-correlates so strongly with the line parameters that it is difficult to constrain their relative contributions to the spectrum.
3. The February-March 1994 OSSE data are consistent with the ASCA results. The 50-150 keV flux is very close to the extrapolation of the ASCA power law. A reflected

power-law component (or a second power law) predicts a slight excess of photons in the OSSE band but is consistent within the uncertainties.

4. The ROSAT PSPC spectra are characterized by strong absorption and steep spectral indices. We interpret this result as indication of soft excess.

5. Flux variability on short (hours) and long (months) time scales is observed in the 0.1-2 keV energy band. Variations of $\sim 30\%$ are also seen by ASCA on time scale of days. The short-time-scale variability is remarkable. While time variability on time scales of days and months had already been seen with the EXOSAT satellite, this is the first time that fast variability on time scale of hours is observed in this source. The short time scale variability, notably the factor 1.2 decrease in the 0.1-2 keV flux in ~ 8000 sec, indicates that the region producing the photons can not be larger than $\sim r_{X\text{-ray}} < ct_D \sim 10^{15}$ cm, where the doubling time scale, $t_D \equiv (F_i/\Delta F)t_{\text{var}}$, is the time necessary for the source flux to change by a factor of two.

6. There is an indication of spectral variability in the soft X-ray range. In particular, the spectral slope increases with intensity, as already noted in 3C 120 (M91) and as is generally observed in Seyfert 1 galaxies (Grandi et al. 1992).

These results indicate that the X-ray emission in 3C 120 is similar to those in radio quite Seyfert galaxies. The excess absorption of soft photons and the soft excess suggested by the ROSAT spectra as well as the well-resolved ASCA iron line exclude a strong contribution of beamed radiation between 0.1 and ~ 8 keV.

3C 120 is not the only case of an intense radio source in which the iron line is seen. Emission features at 6.4 keV have also been detected with ASCA in other radio galaxies, for example, 3C390.3 (Eracleous et al. 1996), 3C445 (Yamashita & Inoue 1996) and 3C109 (Allen et al. 1997). This suggests that the jet intensity in the 0.6-10 keV band is negligible

in at least these radio galaxies. The weakness of the jet contribution can be understood in the framework of unified models if these galaxies are observed at intermediate inclination. In the case of 3C 120, an angle of 15 degrees between the jet axis and the line of sight is sufficiently small to allow superluminal motion of the radio knots to be observed (for bulk velocities $\gamma > 8$) but sufficiently large that the Doppler factor is small, $\delta < 3.0$, so that the intensity of beamed radiation is lower than that within the beam (i.e., at angles $< 1/\gamma < 7^\circ$) by a factor of 20 or more.

What is unusual in 3C 120 is the width and intensity of the iron emission line when the continuum is fitted with a single power law.

We mention two possible explanations for the iron line emission: (1) ASCA can not resolve a hard continuum component (like e.g. a Compton reflection component) and the iron line emission is overestimated. The OSSE observations do not resolve this ambiguity because 3C 120 was very weak in the 50-150 keV band during the simultaneous ASCA-OSSE observation, while OSSE data from literature probably represent the source in a higher state of brightness. In addition the reflection component peaks around 30-40 keV, i.e., in a spectral region not covered by our instruments, while the jet completely dominates the X-ray emission only above 100 keV (see Fig. 4). In any case, the line remains rather broad and intense even if the reflection component is included.

(2) Alternatively, the line is really broad. Martocchia & Matt (1996) have recently investigated the iron fluorescence line emitted by an accretion disc around a rotating (Kerr) black hole. They assume that the X-ray source is isotropic and located on the black hole symmetry axis. Equivalent widths as large as 1-2 keV due to light deflection and gravitational blueshift of the primary radiation are expected if the distance, h , between the X-ray source and the disk is $h < 6r$, where $r = GM/c^2$ is the gravitational radius; i.e., $h < 9 \times 10^{13}$ cm for $M=10^8 M_\odot$. This explanation is not implausible if relativistic jets are

associated with the spin of the black hole rather than with the angular momentum of the accreting matter. However, in this case the line profile is expected to be not only very broad but also significantly redshifted, while the observed redshift, when the line is fitted with a gaussian, is not dramatic.

As any iron line emission is expected to be accompanied by a reflection continuum, the most obvious explanation is actually in term of a line plus the reflection component. Unfortunately, the present data alone do not permit to unambiguously disentangle the two components. We conclude that a Seyfert-like component dominates the X-ray emission of 3C 120 at least in the 0.1-10 keV energy band. To definitively exclude a jet contribution at higher energies requires additional hard X-ray observations.

We thank Tom Bridgman for providing OSSE data in XSPEC format and for the very useful information on the OSSE archive. PG and CMU acknowledge support from NASA grants NAG5-2538 and NAG8-1037. RMS acknowledges financial support from a Research Associate NRC fellowship.

REFERENCES

- Allen, S. W., Fabian, A. C., Idesawa, E., Inoue, H., Kii, T., Otani, C. 1997, MNRAS, in press
- Baldwin, J. A., et al. 1980, ApJ, 236, 388
- Balik, B., Heckman, T. M. 1979, AJ, 84, 302
- Baum, S. A., Heckman, T. M., & van Breugel, W. 1992, ApJ, 398, 208
- Day, C., Arnaud, K., Ebisawa, K., Gotthelf, E., Ingham, J., Mukai, K., & White, N., *The ABC Guide to ASCA Data Reduction*, January 27, 1995
- Elvis, M., Lockman, F. J., & Wilkes, B. J. 1989, AJ, 97, 777
- Eracleous M., Halpern J. P., and Livio M., 1996, ApJ, 459, 89
- Fabian A. C., et al. 1989, MNRAS, 238, 729
- Fiore F., et al. 1994, ApJ, 431, 515
- George, I. M., Fabian, A. C., 1991, ApJ, 368, 167
- Giommi, P., et al. 1990 ApJ, 356,432
- Grandi, P. et al. 1992 ApJS., 82, 93
- Hjorth, J., Vestergaard, M., Sorensen, A. N., Grundahl, F. 1995, ApJ, 452, L17
- Hua, C. T., 1988, A&A 1998, 105
- Iwasawa K., Fabian , A. C., Mushotzky, R. F., Brandt W. N., Awaki H. and Kunieda H., 1996 MNRAS, 279, 846
- Johnson, W. N., et al. 1994, AIP proc., 304, 515
- Kruper J. S., Urry, C. M., Canizares, C. R., 1990, ApJS, 74, 347
- Lightman A.P. & White T. R. 1988, ApJ 335, 57

- Maisack, M., et al. 1995, A&A, 298, 400
- Maraschi L., et al. 1991, ApJ 368, 138 (M91)
- Martocchia, A. & Matt G. 1996, MNRAS, submitted
- Matt, G., Perola, G. G., & Piro, L. 1991, A&A. 267, 643
- Moles, M., del Olmo, A., Masegosa, J., & Perea, J. D. 1988, A&A 197, 1
- Nandra K., George I. M., Mushotzky R. F., Turner T. J., Yaqoob T., 1996a ApJ , inpress
- Nandra K., George I. M., Mushotzky R. F., Turner T. J., Yaqoob T., 1996b ApJ , inpress
- Petre, R., Mushotzky, R. F., Krolik, J. H., & Holt, S. S, 1985, ApJ 280, 499
- Rothschild, R. E., et al. 1983, ApJ , 269,423
- Sambruna R. M. et al. 1994, ApJ 434, 468
- Tadhunter, C. N., Fosbury, P. J., & Quinn, P. J. 1989 MNRAS, 240, 225 Tanaka, Y., Inoue, H., & Holt, S.S. 1994, PASPJ, 46, L37
- Treves A., et al. 1988, ApJ, 330, 178
- Turner, T. J., et al. 1991, ApJ, 381, 85
- von Montigny, C., et al. 1995 A&A 299,680
- Walker, A.C., Benson, J. M., & Unwin, S. C. 1987, ApJ, 316, 546
- White, N. E., Giommi, P., & Angelini, L. 1994, BAAS, 185, 41.11
- Yamashita, A. & Inoue, H. 1996, Abstracts of *X-ray Imaging and Spectroscopy of Cosmic Hot Plasmas - International Conference on X-ray Astronomy - ASCA 3rd Anniversary*, pag. 75
- Zenzus, J. A., 1989, in Lecture Notes in Physics, Vol. 334, BL Lac Objects, ed. L. Maraschi, T. Maccacaro & M-H Ulrich (Berlin: Springer), 3

Figure Captions

Figure 1. Light curves a) in the SIS0+SIS1 detectors (0.5-8 keV) and b) in the GIS2+GIS3 detectors (1-10 keV). The bin size is 500 sec. Significant variability with amplitude $\sim 30\%$ is present on time scales of half a day.

Figure 2. Ratio of a) SIS and b) GIS data to model for power-law fit. An excess of emission is clearly evident at ~ 6.2 keV.

Figure 3. Iron line width versus iron line normalization at 68%, 90% and 99% confidence contour levels for a power law (Γ free to vary) plus gaussian profile model.

Figure 4. Confidence contours in the two fit parameters, the amount of reflection (R) and the intrinsic width (σ_{Fe}) of the iron line, for the GIS2+GIS3 data. Contours represent 68%, 90% and 99% confidence levels. The strong anti-correlation between the two parameters is evident.

Figure 5. ASCA–OSSE spectrum of 3C 120. The filled circle represents the contemporaneous February–March 1994 OSSE observations; the open circle is an average from published OSSE data. The OSSE data are best fitted by an extrapolation of the single ASCA power law (which implies a broad iron line) or the reflection component. The extrapolation of a second, flatter power law, which fits the non-contemporaneous high state OSSE data very well, may indicate that the jet component is highly variable and is significant only at higher intensities.

Figure 6. ROSAT light curves for the observations of 10 September 1993. The bin size is 400 s. A clear decrease in intensity, with doubling time ~ 6 hours, is seen.

Table 1: Journal of Observations

| Satellite | Instrument | Date | Count Rate (sec ⁻¹) | error | F _ν ^a (μJy) |
|-----------|-------------------|-------------------|------------------------------------|-------|---|
| ROSAT | PSPC | 1993 Mar 6 | 1.740 | 0.030 | 10.76 ^{+1.73} _{-1.30} |
| | | 1993 Aug 25 | 3.010 | 0.038 | 23.98 ^{+4.12} _{-3.25} |
| | | 1993 Sep 2 | 2.040 | 0.030 | 14.02 ^{+2.19} _{-1.73} |
| | | 1993 Sep 10 | 2.413 | 0.035 | 14.28 ^{+2.46} _{-1.53} |
| ASCA | SIS0 | 1994 Feb 17–19 | 1.861 | 0.006 | 11.03 ^{+0.25} _{-0.24} |
| | | | 1.412 | 0.006 | |
| | | | 0.905 | 0.005 | |
| | | | 1.095 | 0.006 | |
| GRO | OSSE ^b | 1994 Feb 17–Mar 1 | 0.087 | 0.31 | 1.32 ± 0.47 × 10 ⁻³ |
| | | 1994 Mar 1–8 | | | |

^a - ν=1 keV for ASCA and ROSAT; ν=100 keV for OSSE

^b - Average count rate and flux density from both the two OSSE observations

Table 2: ASCA Time Variability

| Instrument | Bin size | $\chi^2/\text{d.o.f}$ |
|------------|----------|-----------------------|
| | sec | |
| SIS0 | 100 | 376/180 |
| | 500 | 154/34 |
| | 1000 | 66/5 |
| SIS1 | 100 | 367/177 |
| | 500 | 176/33 |
| | 1000 | 69/5 |
| GIS2 | 100 | 490/176 |
| | 500 | 122/49 |
| | 1000 | 64/14 |
| GIS3 | 100 | 294/174 |
| | 500 | 134/49 |
| | 1000 | 69/14 |

Table 3: Fits to ASCA Spectrum of 3C 120 : 0.6-10 keV Energy Band

| Model ^a | Γ_1 | N_H (10^{21} cm^{-2}) | E_{Fe} (keV) | σ_{Fe} (keV) | EW (eV) | Γ_2 | E_{break} (keV) | R | $\chi^2_{\nu}(d.o.f)$ |
|------------------------------|------------------------|--|--|------------------------|---------------------------------------|------------------------|-----------------------------|------------------------|-----------------------|
| SIS0+SIS1 (0.6-5 keV) | | | | | | | | | |
| PL | 2.00 ± 0.02 | 1.64 ± 0.07 | | | | | | | 1.11(66) |
| SIS0+SIS1 (0.6-8 keV) | | | | | | | | | |
| PL | $1.96^{+0.01}_{-0.02}$ | 1.52 ± 0.06 | | | | | | | 1.53(128) |
| PL+GA | 2.00 | $1.63^{+0.04}_{-0.03}$ | $6.06^{+0.22}_{-0.20}$ | $0.80^{+0.25}_{-0.19}$ | 357^{+111}_{-72} | | | | 1.11(126) |
| PL+GA | 2.00 ± 0.02 | 1.65 ± 0.07 | $6.06^{+0.26}_{-0.21}$ | $0.82^{+0.28}_{-0.21}$ | 399^{+133}_{-122} | | | | 1.11 (125) |
| PL+DISKL ^b | 2.00 | $1.66^{+0.03}_{-0.04}$ | 6.2 | 0.4 | 151^{+56}_{-41} | | | | 1.39(128) |
| PL+2GA | 2.00 | $1.65^{+0.04}_{-0.03}$ | $5.27^{+0.08}_{-0.05}$ 6.20 ± 0.1 | 0.1 0.1 | 70^{+25}_{-36} 107^{+35}_{-42} | | | | 1.34(125) |
| BK+GA | 2.00 | $1.64^{+0.03}_{-0.04}$ | 6.2 | 0.4 | 114 ± 64 | 1.79 ± 0.09 | $4.20^{+0.33}_{-0.41}$ | | 1.14(126) |
| BK+GA | 2.00 | $1.64^{+0.04}_{-0.03}$ | 6.2 | 0.4 | 140^{+50}_{-88} | 1.83 ± 0.07 | 4.00 | | 1.14(127) |
| BK+GA | 2.00 | 1.63 ± 0.03 | $5.98^{+0.31}_{-0.28}$ | $0.67^{+0.36}_{-0.27}$ | 244^{+311}_{-137} | $1.92^{+0.21}_{-0.12}$ | 4.00 | | 1.11(125) |
| PLREF+GA | 2.00 | 1.62 ± 0.04 | 6.2 | 0.4 | 171^{+50}_{-86} | | | $0.82^{+0.47}_{-0.48}$ | 1.19(127) |
| PLREF + GA | 2.00 | $1.63^{+0.04}_{-0.03}$ | $6.06^{+0.26}_{-0.22}$ | $0.80^{+0.25}_{-0.21}$ | 372^{+94}_{-133} | | | $0.00 < 0.53$ | 1.12(125) |
| GIS2+GIS3 (1-10 keV) | | | | | | | | | |
| PL | 1.87 ± 0.03 | $0.73^{+0.28}_{-0.27}$ | | | | | | | 1.31(174) |
| PL+GA | 2.00 | 1.53 ± 0.16 | $6.31^{+0.19}_{-0.24}$ | $0.93^{+0.25}_{-0.20}$ | 674^{+129}_{-144} | | | | 0.93(172) |
| PL+GA | $2.02^{+0.08}_{-0.05}$ | $1.68^{+0.49}_{-0.41}$ | $6.30^{+0.20}_{-0.19}$ | $1.01^{+0.44}_{-0.28}$ | 764^{+456}_{-251} | | | | 0.93(171) |
| BK+GA | 2.00 | 1.53 ± 0.16 | 6.2 | 0.4 | 222^{+55}_{-82} | 1.78 ± 0.08 | $3.99^{+0.44}_{-0.50}$ | | 0.92(172) |
| BK+GA | 2.00 | $1.52 < 0.16$ | 6.24^{+24}_{-20} | $0.65^{+0.01}_{-0.34}$ | 332^{+229}_{-161} | $1.84^{+0.12}_{-0.10}$ | 4.00 | | 0.91(171) |
| PLREF+GA | 2.00 | 1.41 ± 0.15 | 6.2 | 0.4 | 222^{+56}_{-92} | | | $1.60^{+0.61}_{-0.62}$ | 0.98(173) |
| PLREF+GA | 2.00 | $1.49^{+0.19}_{-0.18}$ | 6.30 ± 0.20 | $0.85^{+0.30}_{-0.31}$ | 527^{+240}_{-246} | | | $0.44 < 1.52$ | 0.93(171) |

Table 3: - continued

| Model ^a | Γ_1 | N_H (10^{21} cm^{-2}) | E_{Fe} (keV) | σ_{Fe} (keV) | EW (eV) | Γ_2 | E_{break} (keV) | R | $\chi^2_{\nu}(d.o.f)$ |
|---|------------|--|------------------------|------------------------|--------------------|------------------------|-----------------------------|---------------|-----------------------|
| SIS0+SIS1+GIS2+GIS3 (0.6-10 keV) | | | | | | | | | |
| PL+GA | 2.00 | $1.62^{+0.04}_{-0.03}$ | $6.23^{+0.16}_{-0.15}$ | $0.89^{+0.17}_{-0.15}$ | 509^{+67}_{-85} | | | | 1.02(302) |
| BK+GA | 2.00 | $1.62^{+0.04}_{-0.03}$ | 6.14 ± 0.18 | $0.69^{+0.23}_{-0.24}$ | 278^{+159}_{-78} | $1.88^{+0.10}_{-0.08}$ | 4.00 | | 1.012(301) |
| PLREF+GA | 2.00 | $1.62^{+0.04}_{-0.03}$ | $6.23^{+0.16}_{-0.15}$ | $0.89^{+0.16}_{-0.15}$ | 497^{+77}_{-120} | | | $0.00 < 0.42$ | 1.025(301) |

^a PL=Power Law - GA=Gaussian line - BK=Broken Power Law - PLREF=Reflection Model - DISKL= Gravitational shifted line profile

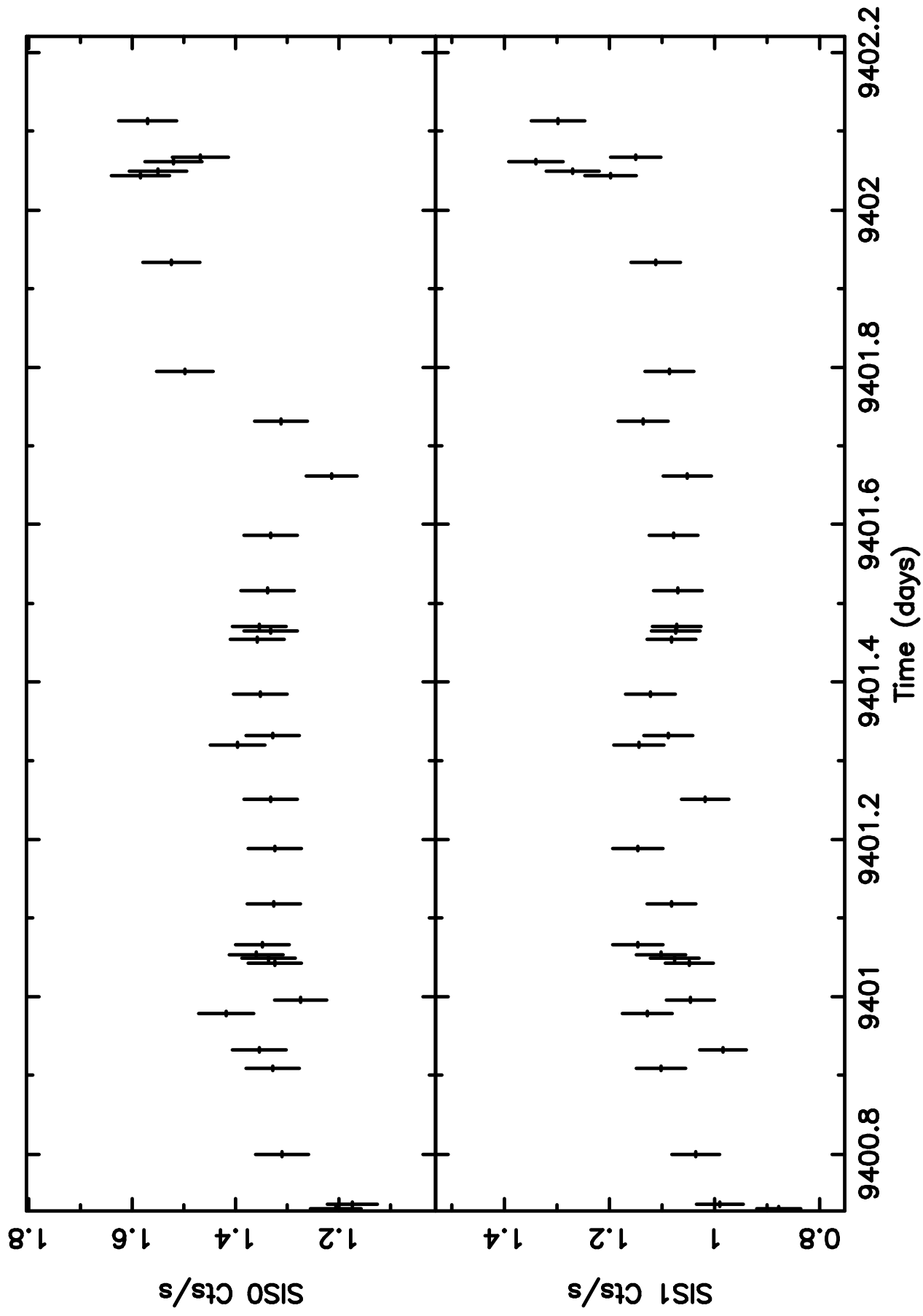
^b The inclination of the disk is fixed to the value $i=15^\circ$

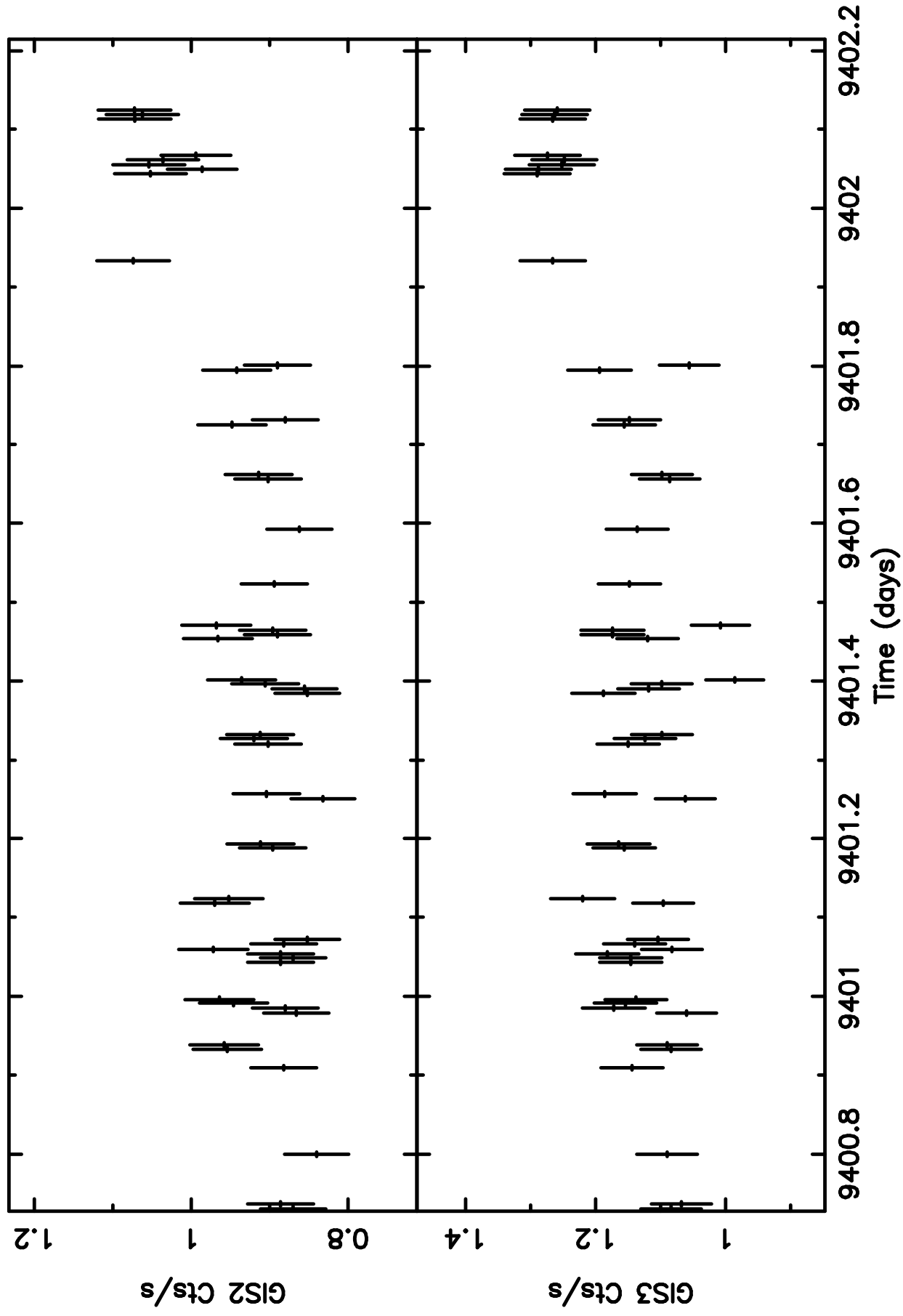
Table 4: ROSAT Results: Power Law Model

| Date | N_H | Γ | $\chi_r^2(\text{d.o.f})$ |
|--------------|-------------------------------|------------------------|--------------------------|
| | (10^{21} cm^{-2}) | | |
| 1993 Mar 6 | $2.26^{+0.53}_{-0.43}$ | $2.54^{+0.32}_{-0.28}$ | 1.09(124) |
| 1993 Aug 25 | $3.12^{+0.55}_{-0.50}$ | $3.27^{+0.34}_{-0.31}$ | 1.15(137) |
| 1993 Sept 2 | $2.58^{+0.50}_{-0.44}$ | $2.95^{+0.31}_{-0.29}$ | 1.02(140) |
| 1993 Sept 10 | $2.11^{+0.54}_{-0.38}$ | $2.78^{+0.34}_{-0.27}$ | 1.12(127) |

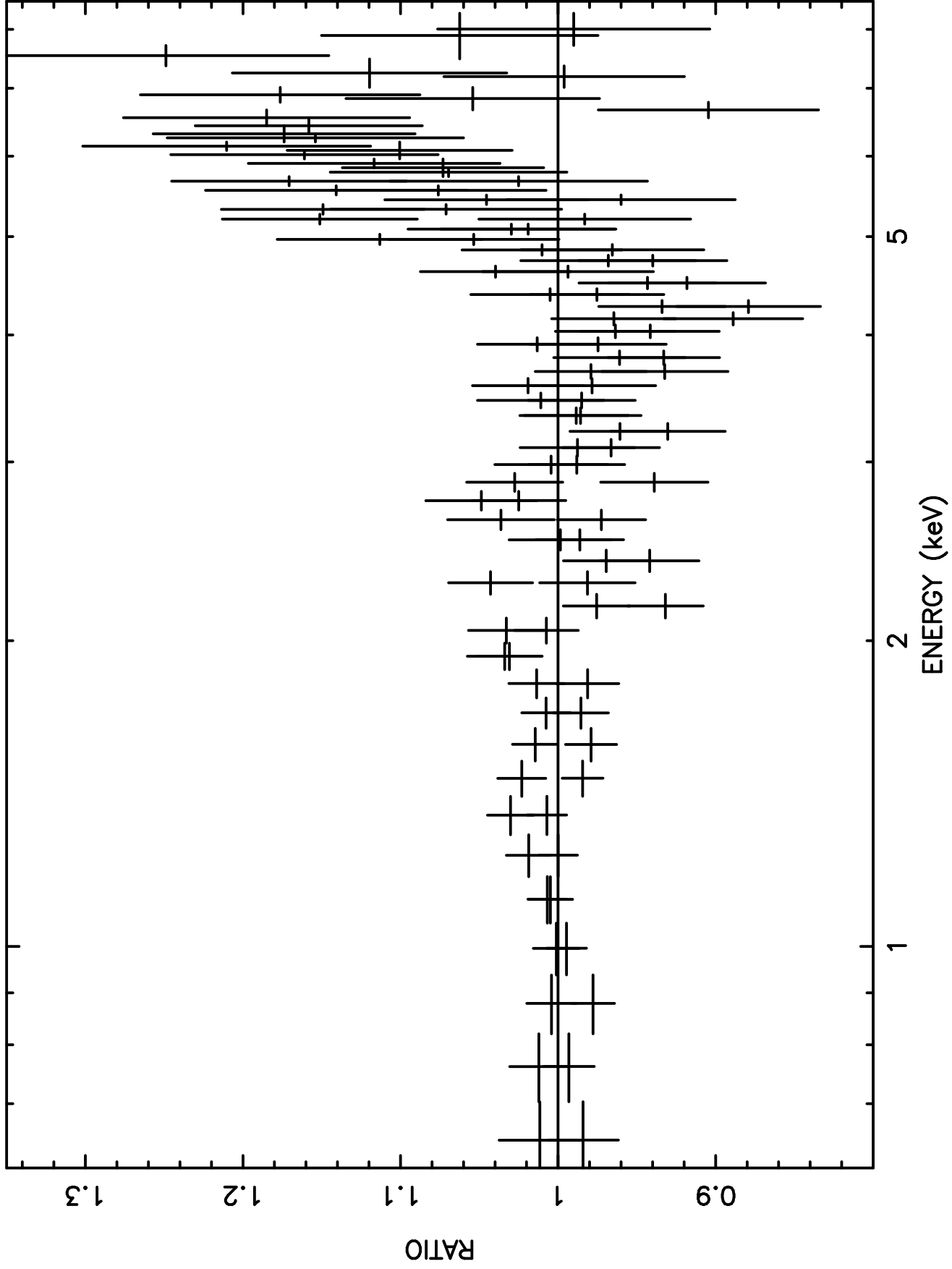
Table 5: ROSAT Results: Power law + Raymond-Smith Model

| Date | Γ | kT | $\chi_r^2(\text{d.o.f})$ |
|--------------|------------------------|------------------------|--------------------------|
| | | (keV) | |
| 1993 Mar 6 | $1.55^{+0.15}_{-0.18}$ | $0.62^{+0.18}_{-0.23}$ | 1.13(123) |
| 1993 Aug 25 | $1.79^{+0.15}_{-0.12}$ | $0.80^{+0.08}_{-0.13}$ | 1.32(136) |
| 1993 Sept 2 | $1.79^{+0.12}_{-0.12}$ | $0.68^{+0.16}_{-0.13}$ | 1.08(139) |
| 1993 Sept 10 | $1.96^{+0.12}_{-0.13}$ | $0.67^{+0.20}_{-0.24}$ | 1.17(126) |

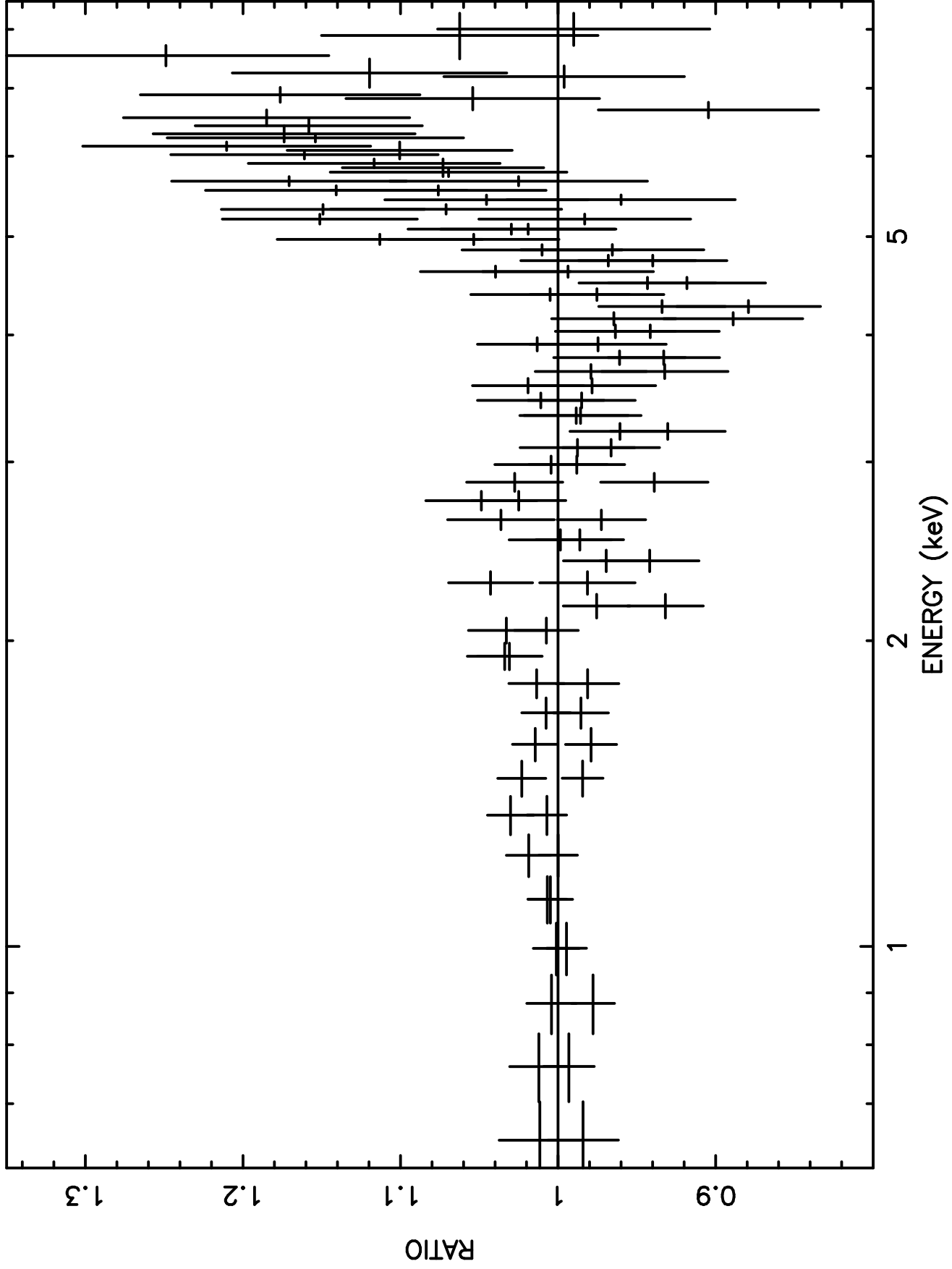




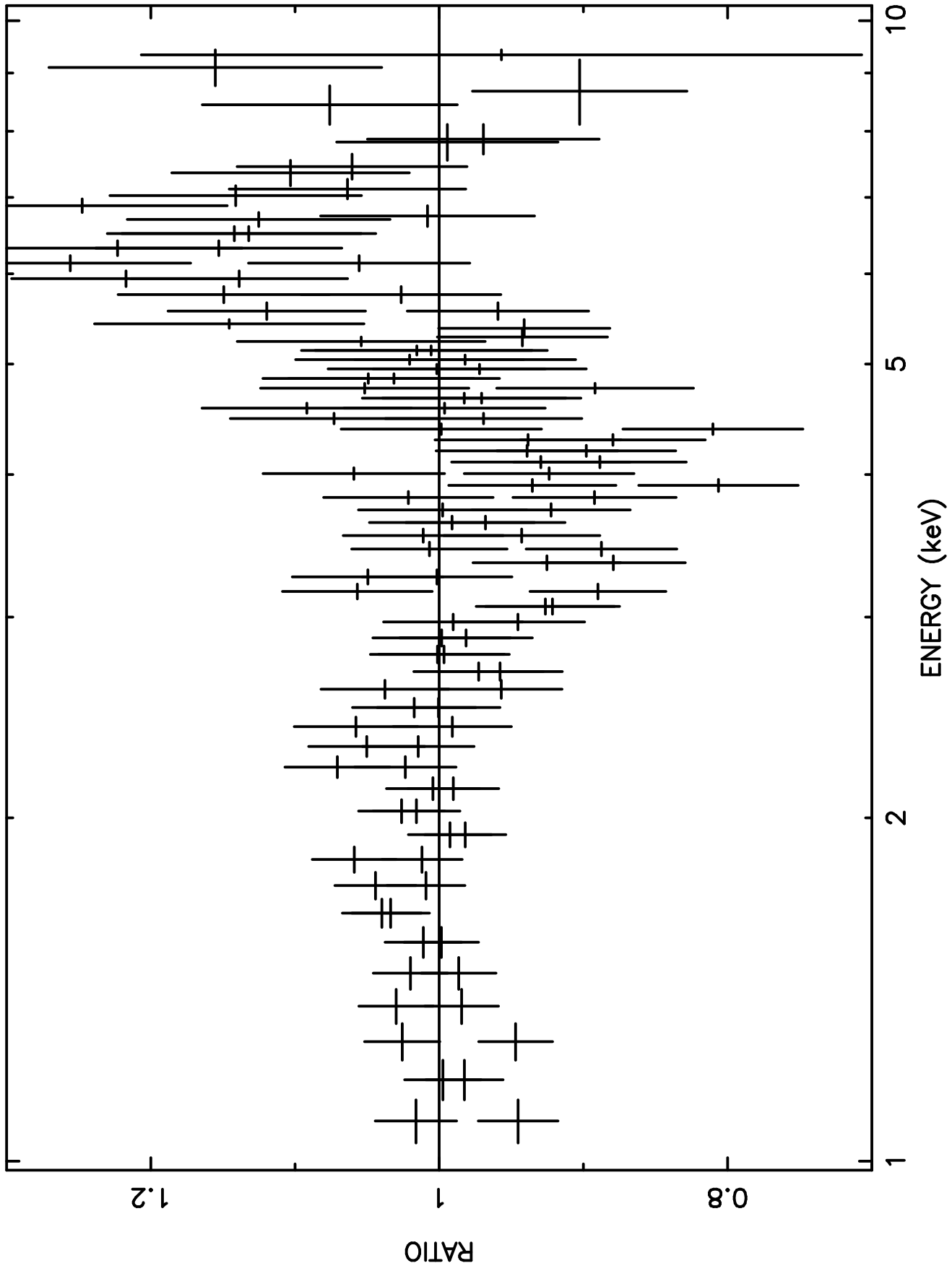
SIS0 + SIS1: ABSORBED POWER LAW

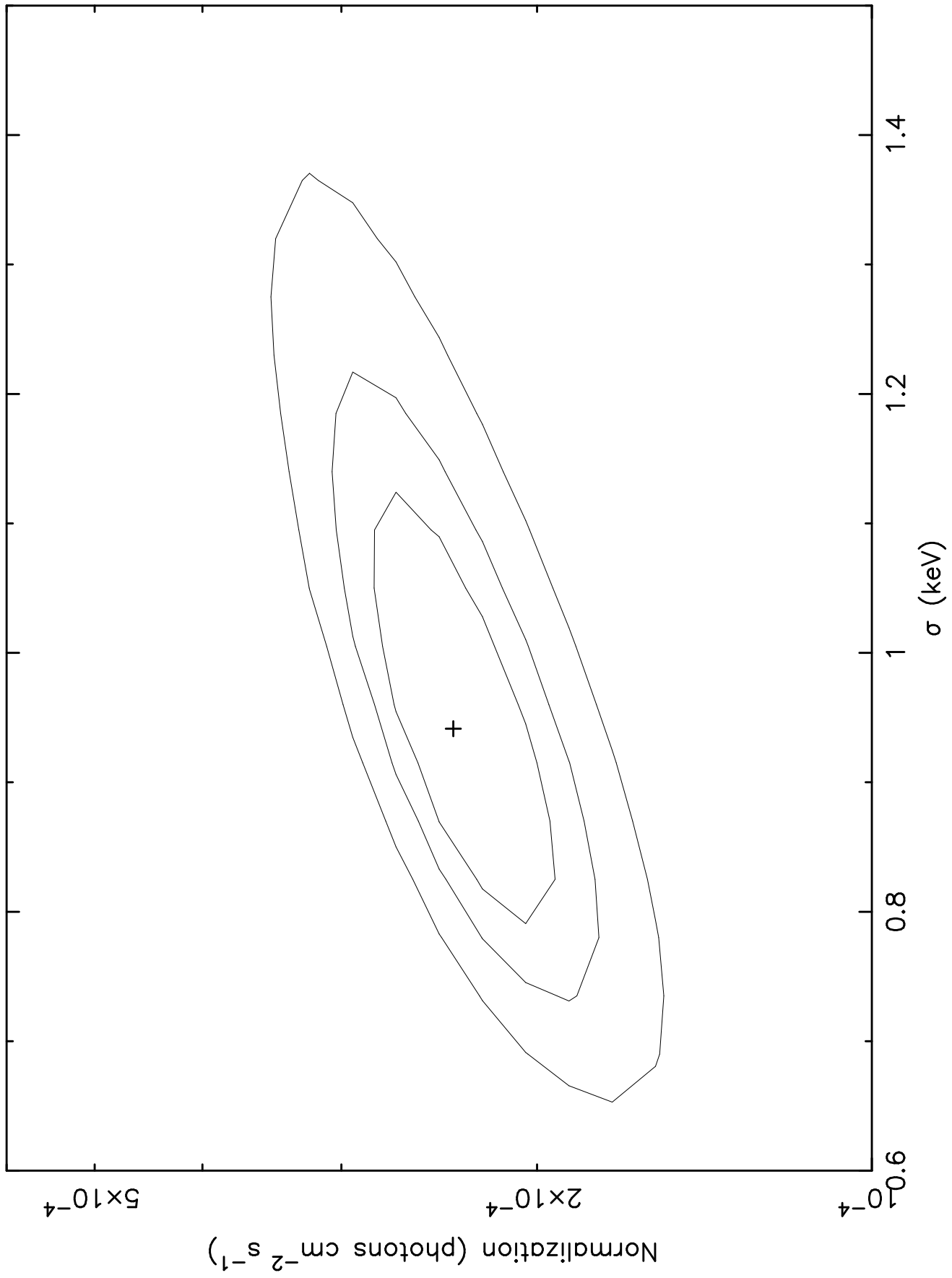


SIS0 + SIS1: ABSORBED POWER LAW

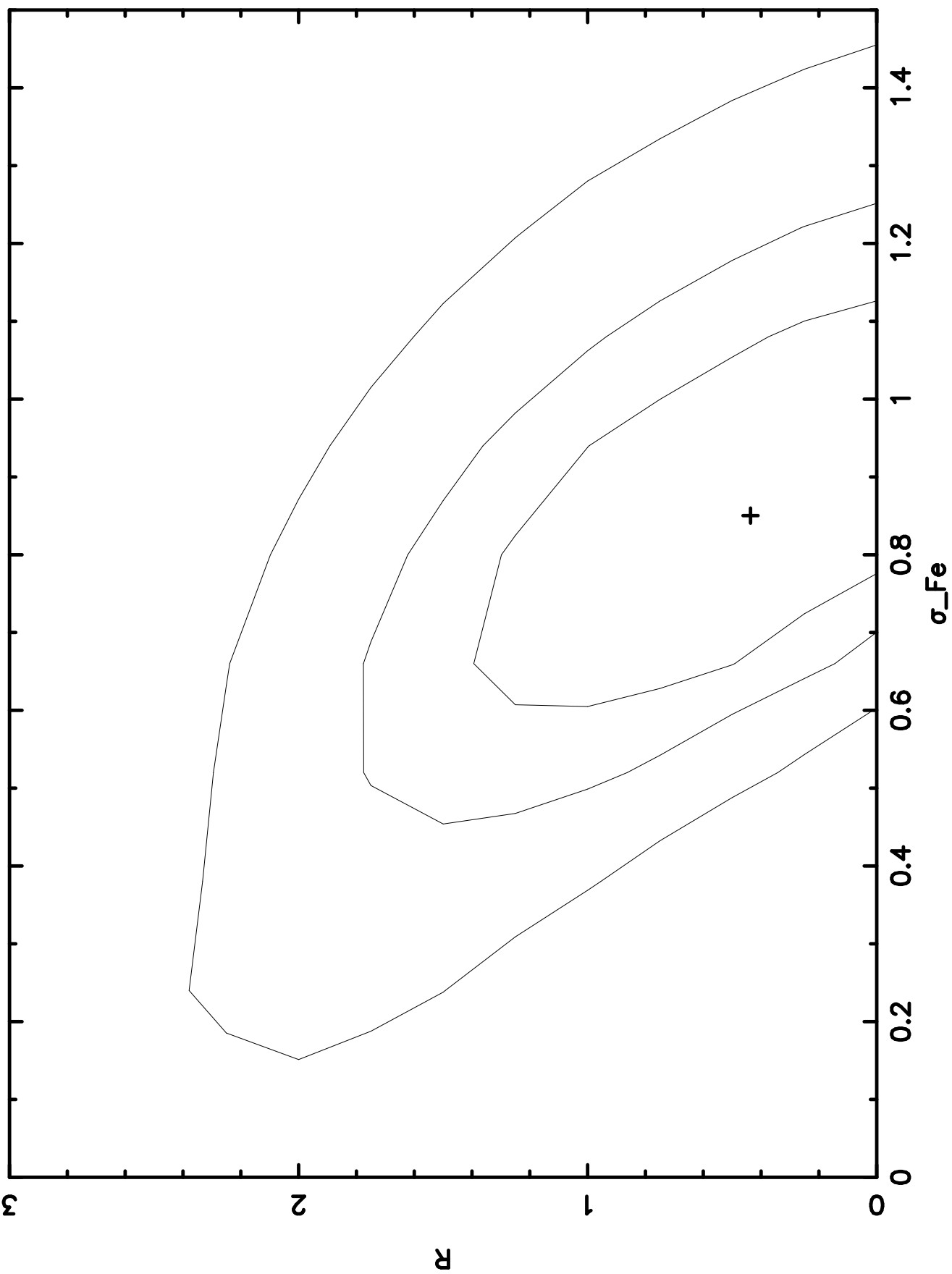


GIS2 + GIS3: ABSORBED POWER LAW

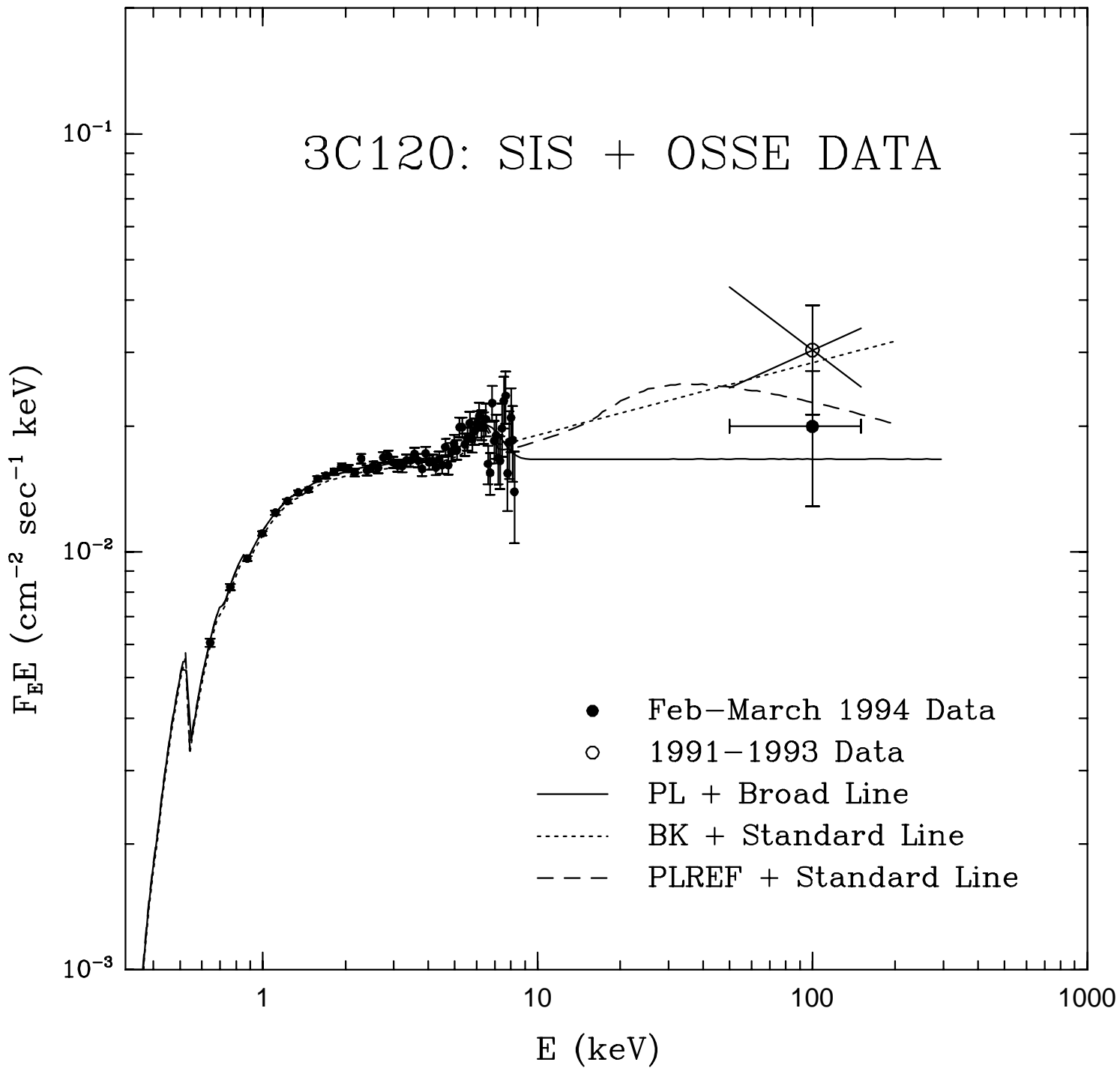




Confidence contours



3C120: SIS + OSSE DATA



3C 120: ROSAT PSPC Light Curve of 10 September 1993

